Journal of Marine Research, 44, 521-542, 1986

A model study of the seasonal cycle of the Arabian Sea surface temperature

by Satish R. Shetye[1]

ABSTRACT

The Annual variation of the SST along a zonal strip from the coast of Somalia to the southwest coast of India was simulated using available data (monthly-mean heat and momentum fluxes across the air-sea interface, surface advective field, etc.) as input to a Kraus-Turner mixed-layer model. Three cases were examined. In the first, influence of surface fluxes alone was considered. The second included the effects of surface fluxes and vertical advection. Then, effect of horizontal advection was added.

The model forced with the surface heat and momentum fluxes alone simulated reasonably well the SST variability throughout the year except during the May–August (southwest monsoon) cooling phase. The model was found to be inadequate to handle the coastal areas during this phase. Over the open-sea regime the performance of the model was better; and, it improved when the influence of advection was included. The important contribution of the horizontal advection during June–August was to remove most of the heat gained at the surface during the course of a year. Though downwelling in the open-sea had little influence on the SST, it had noticeable impact on the vertical heat transport.

The numerical experiments suggest that the Kraus-Turner thermodynamics alone dominate the Arabian SST variability throughout the year except during the southwest monsoon, when dynamics too play a significant role.

1. Introduction

The annual march of the Arabian Sea surface temperature (ASST) shows the following four phases (Colborn, 1976): (1) a warming phase from approximately February to May; (2) cooling from May to August; (3) warming from September to mid-November; and, (4) cooling from mid-November to January. This behavior is in contrast to the annual march of the SST over most of the other regions of the world oceans, which show only two phases: warming during the fair weather period of spring and summer; and, cooling during fall and winter, the foul weather period.

All available evidence suggests that the abnormal behavior of the Arabian Sea (AS) is due to the influence of the southwest (SW) monsoon which dominates the AS during the Northern Hemisphere summer. The energetic wind circulation during this season is believed to influence the ASST in the following ways. In the coastal areas upwelling

1. Physical Oceanography Division, National Institute of Oceanography, Dona-Paula, Goa 403004, India.

brings up cooler water which then spreads offshore (Duing and Leetmaa, 1980). In the open sea, entrainment and heat loss at the surface reduce the SST. It is not known which of these processes contributes most to the SST variability. Other aspects of the ASST variability not understood at the present include the following. The AS is a region of net annual heat gain at the surface. The annual cycle of the thermal structure can therefore be maintained only if this heat is removed. How and when this is achieved is not understood. The SW monsoon circulation over the AS is marked by the presence of a strong curl of the wind stress field. Such a field can be expected to influence the vertical transport of heat in the upper ocean. The effect of this on the SST is not known. Added recent interest in the ASST stems from the suggestion that the pattern of anomalies of the ASST influences the precipitation pattern of the SW monsoon over India (Shukla, 1975; Washington *et al.*, 1977; Druyen *et al.*, 1983).

Almost all the information relevant to the study of the ASST comes from two types of sources. The first and the more extensive of these is the maritime data. Monthly-mean values of SST, surface winds, air-sea fluxes, etc. compiled by using such data have been summarized in atlases. The second source is the collection of hydrocasts and XBT casts. These are few, and the monthly-mean picture based on them has been summarized in Colborn (1976). The annual cycle of the thermal field in the upper Arabian Sea has been revealed through these monthly-mean values alone. No data of the kind provided by weather ships in the Atlantic and the Pacific (Denman and Miyake, 1973; Gill and Turner, 1976) are available in the AS.

No attempt has yet been made to model the annual cycle of the ASST. The work reported here is a step in this direction. Here we put together a zero-order, but nonetheless a comprehensive and quantitative, description of the annual cycle of the ASST by: (1) assembling the available climatological monthly-mean data that are pertinent to the behavior of the ASST, and (2) carrying out numerical experiments with a model for the AS mixed-layer.

Most of the data for this study are derived from the two atlases by Hastenrath and Lamb (1979a, b), hereafter referred to as HL1 and HL2. HL1 gives 60-year monthly-mean values of SST and of surface wind field over the Indian Ocean. HL2 describes monthly-mean heat fluxes over the same ocean. In addition to these, data on ship-drift estimates given in KNMI Atlas (1952) have been used. For the sake of brevity, not the whole of the AS has been examined. Attention is restricted to a 2° latitude zonal strip, centered at 10N and stretching from the coast of Somalia to the southwest coast of India. The strip, shown in Figure 1, has been divided into 13 areas, each of 2° longitudinal extent. The strip has the intense upwelling region of the Somalia coast on its western edge (Area 1), the typical open-sea regime in the central portion (Areas 3–9), region dotted by islands of the Lakshadweep Archipelago (Areas 10–12), and another upwelling regime, though on a scale much weaker than the one off Somalia, on its eastern edge (Area 13). The strip therefore contains samples of a variety of regimes that are expected to be important in understanding the AS mixed-layer.

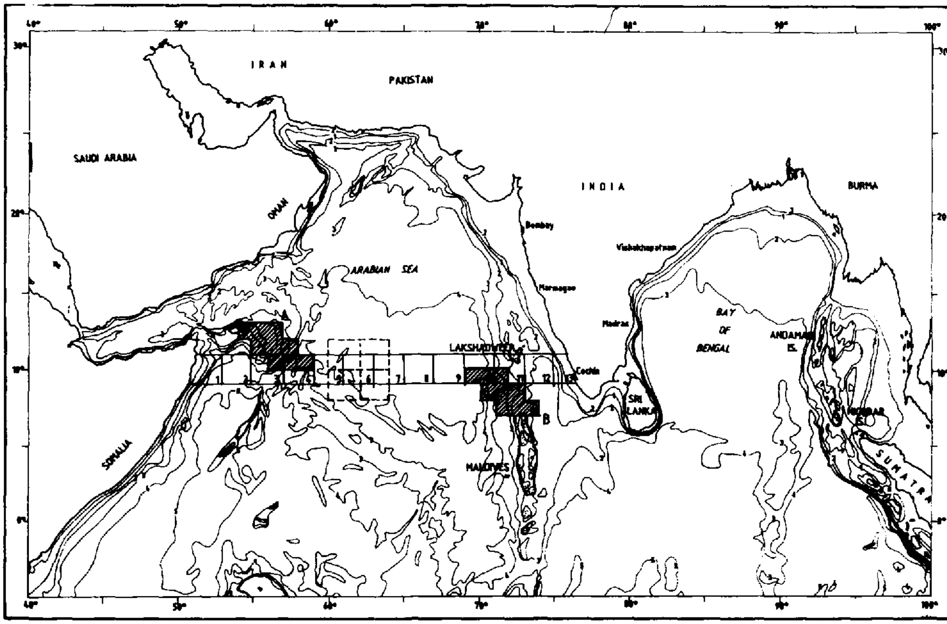

Figure 1. The area of interest. The 9–11N strip over which the behavior of the mixed-layer has been studied stretches from the coast of Somalia to the southwest coast of India. The strip has been divided into 13 areas. The hatched regions A and B are explained in Section 3. The four 2°-squares surrounding Area 6 of the strip are explained in Section 4.3. The bathymetric contours are in kilometers.

The theoretical model used here is based on the ideas pioneered by Kraus and Turner (1967), and incorporates parameterization schemes that have been found successful in simulating the seasonal variation of the mixed-layer in other parts of the world oceans. In the next section we describe the model. In Section 3 the climatological data over the 10N strip are described. Section 4 discusses the results of the numerical experiments. Conclusions are summarized in Section 5.

2. The model

We use a modified version of the Denman (1973) implementation of the mixed-layer model of Kraus and Turner (1967). It is assumed that the surface layer is homogeneous up to a depth h with temperature T_s. At the bottom of the homogeneous regime there occurs a discontinuity where the temperature drops from T_s to T_{-h}. Below the discontinuity the temperature changes at a prescribed rate given by $(\partial T/\partial z)_{-h}$. A schematic mixed-layer is shown in Figure 2 which also summarizes the processes that the model takes into account. They include the following: (1) Effect of momentum flux into the mixed-layer due to action of wind stress τ (dyne/cm^2) on the air-sea interface. (2) Heating of the mixed-layer by penetrative shortwave solar radiation. Strength of

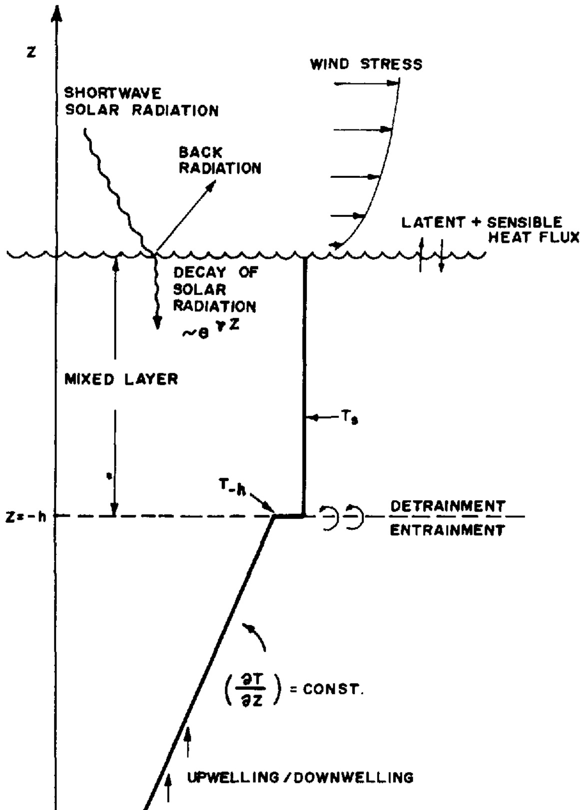

Figure 2. Taken from Denman (1973), the figure summarizes the processes included in the model. The vertical temperature profile consists of a homogeneous mixed-layer of thickness h and temperature T_s, followed by a temperature discontinuity $(T_s - T_{-h})$, and a region with temperature gradient $(\partial T/\partial z)_{-h}$. The surface fluxes are: wind stress (τ); incoming solar radiation (S_*); back radiation $(-B_*)$; the latent heat and the sensible heat flux together given by $-(He_* + Hs_*)$. The solar radiation decays in the mixed-layer as $e^{\nu z}$. A vertical velocity (w) is prescribed below the mixed-layer.

the radiation at the air-sea interface is R_* (cal cm^{-2} sec^{-1}). It is assumed that this radiation decays exponentially on propagating into the mixed-layer with extinction coefficient ν (cm^{-1}), and that no radiation penetrates below the homogeneous regime into the thermocline. (3) Cooling of the mixed-layer due to loss of heat from longwave back radiation at the surface B_* (cal cm^{-2} sec^{-1}). (4) Effect of the heat loss/gain due to turbulent heat fluxes at the surface such as the sensible heat flux Hs_* (cal cm^{-2} sec^{-1}) and the latent heat flux He_* (cal cm^{-2} sec^{-1}). (5) Effect of entrainment of the colder water from the thermocline into the homogeneous layer. (6) Effect of detrainment which occurs when the mixed-layer shallows.

We refer the reader to Denman (1973) for a detailed discussion of how the above processes are incorporated into the model equations that describe the evolution of h and T_s with time t. Here it suffices to state the equations:

$$\frac{dT_s}{dt} = \frac{2}{h^2}\left[-\frac{1}{\zeta_0\bar{\alpha}g}(G_* - D_*) + \frac{h}{\zeta_0 C_p}T_* - \frac{R_*}{\nu\zeta_0 C_p}(1 - e^{-\nu h})\right], \tag{1}$$

$$H\left(\frac{dh}{dt}\right) = \frac{1}{h(T_s - T_{-h})}\left\{\frac{2}{\zeta_0\bar{\alpha}g}(G_* - D_*) + \frac{R_*}{\zeta_0 C_p}\left[\frac{2}{\nu}(1 - e^{-\nu h}) - he^{-\nu h}\right] - \frac{h}{\zeta_0 C_p}T_*\right\} \tag{2}$$

$$\frac{dT_{-h}}{dt} = -\frac{dh}{dt}\left(\frac{\partial T}{\partial z}\right)_{-h}. \tag{3}$$

C_p is the specific heat of water (cal/(gm °C)), ζ_0 the mean density of water, and g the acceleration due to gravity. $\bar{\alpha}$ is the modulus of the coefficient of expansion of water (1/°C). T_* is the total downward heat flux across the air-sea interface ($T_* = R_* + Hs_* + He_* + B_*$). H in Eq. (2) is the Heaviside step function. The left-hand side of this equation equals (dh/dt) when τ increases due to entrainment and is zero when h decreases due to detrainment. G_*–D_* is the function that determines generation minus dissipation of the turbulent kinetic energy. In the present model we use the following form for this function:

$$G_* - D_* = \eta\zeta_0\left(\frac{\tau}{\zeta_0}\right)^{3/2} - \zeta_0\epsilon_m h \quad \text{if } T_* > 0 \tag{4a}$$

$$= \eta\zeta_0\left(\frac{\tau}{\zeta_0}\right)^{3/2} - \zeta_0\epsilon_m h + \frac{0.85}{2}\frac{g\bar{\alpha}}{C_p}T_* h \quad \text{if } T_* < 0 \tag{4b}$$

Eq. (4a) concerns the condition when the ocean gains heat at the surface. The first term represents the kinetic energy generated by the action of the wind stress τ, η being the parameter which relates the two. The second term represents the background dissipation, ϵ_m being the coefficient of dissipation. This term was introduced by Alexander and Kim (1976), who found that in its absence the computed mixed-layer depth was very much in excess of the observed depth. The last term on the right-hand side of Eq. (4b) ensures that potential energy is lost when the surface is cooled. This term was added following Gill and Turner (1976), who chose the constant, 0.85, to fit observations. The equation for ($G_* - D_*$) in the form written above was suggested by Kim (1976).

Eqs. (1–4) do not take into account the effect of vertical and horizontal advection. Denman (1973) has shown that the influence of the vertical velocity, w, in the thermocline can be incorporated in Eqs. (1) to (3) by replacing (dh/dt) by ($dh/dt + w$) on the left-hand side of Eq. (2) and on the right-hand side of Eq. (3). The rate of temperature change produced by horizontal advection depends on $\mathbf{u} \cdot \nabla T_s$ where $\mathbf{u}$ is the horizontal velocity. Its influence can be incorporated into the model by adding $\mathbf{u} \cdot \nabla T_s$ to the left-hand side of Eq. (1).

In the numerical experiments carried out here we shall first examine the SST variation due to the influence of the surface fluxes alone. Then, the combined effect of the surface fluxes and the vertical advection will be examined. While doing so w will be assumed to be externally specified. Finally, the influence of all three—the surface fluxes, the horizontal and the vertical advection will be looked at. In this case, $\mathbf{u} \cdot \nabla T_s$ too is externally specified using observed monthly mean values for $\mathbf{u}$ and for T_s.

All experiments were started with a simple initial temperature profile based on observations. The evolution of this profile with time was predicted using the model. The history of evolution was kept track of by storing selected profiles with a resolution of 1 m. In the model it is assumed that the temperature below the homogeneous surface layer is not affected by the surface fluxes, but is influenced by vertical and horizontal advection. The role of vertical advection is to move the profile below the mixed-layer vertically with a velocity equal to w. The role of horizontal advection is to change the temperature at a rate equal to $-\mathbf{u} \cdot \nabla T_s$ (see Sections 4.2 and 4.3 for details).

3. Data

The annual march of the monthly-mean SST along the 10N strip is shown in Figure 3. Two observations are evident from the figure. Firstly, the SST always increases from the west to the east. Secondly, the SST goes through four well-marked cooling/warming phases during a year. The latter is better brought out in Figure 4 which gives the rate of change of temperature (°C/month) of the strip.

The monthly-mean resultant wind field in the AS is summarized in charts 14–25 of HL1. We computed the monthly-mean wind stress by using the following expression:

$$\tau = C_D \zeta_a \left(1 + \frac{\sigma^2}{\overline{V}^2}\right) \overline{V}^2$$

ζ_a is the density of air (gm/cm^3), C_D the drag coefficient, $\overline{V}$ the monthly-mean scalar wind (resultant wind divided by steadiness) and σ is the standard deviation of the scalar wind during the month. C_D given in Kondo (1975) has been used. Monthly-mean steadiness values given in US Navy Marine Climatic Atlas (1976) for two areas A and B shown in Figure 1 have been used. As wind stress depends on the square of the scalar wind, monthly-mean stress ought to be computed using monthly-mean value of the square of the scalar wind. If computed from the monthly-mean scalar wind instead, the factor in the bracket needs to be included. σ has been assigned a value of 1.15 m/s. This figure is based on Table 4 in HL1. The computed wind stress field is shown in Figure 5. The most prominent signal in the figure arises due to the SW monsoon.

The annual march of the net shortwave radiation over the 10N strip is shown in Figure 6 which is based on charts 2–13 of HL2. During the SW monsoon the variability of the radiation is closely linked to the extent of the cloud cover that persists over the AS. The western edge of the strip has cooler SST's, which make the

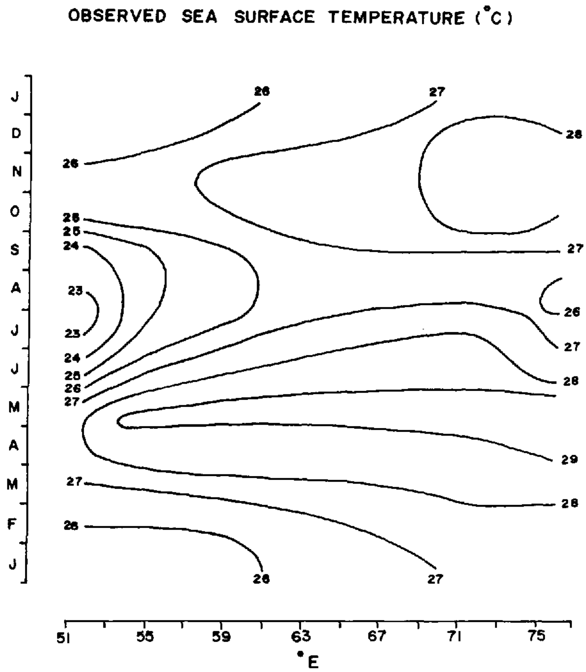

Figure 3. Contours showing the observed SST (°C). The horizontal axis gives the distance along the 10N strip shown in Figure 1. The vertical axis defines the month of the year.

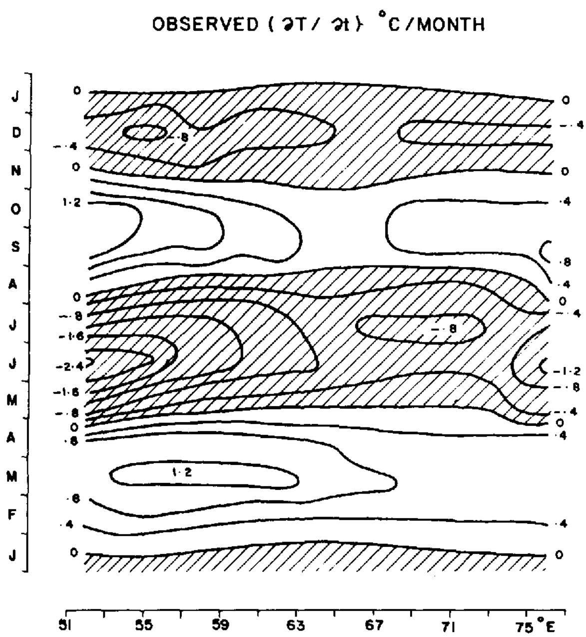

Figure 4. Observed rate of change in temperature (°C/month). The negative rates of change are shown hatched.

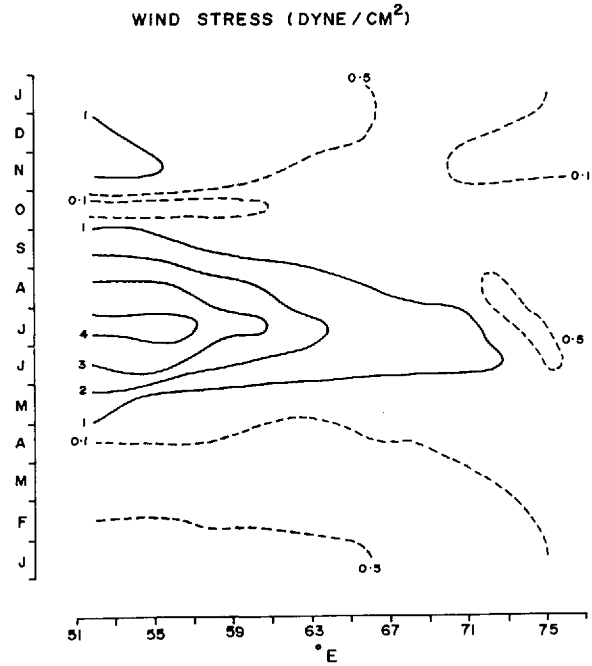

Figure 5. Wind stress (dyne/cm^2). Contours below 1 dyne/cm^2 are shown by dashed lines.

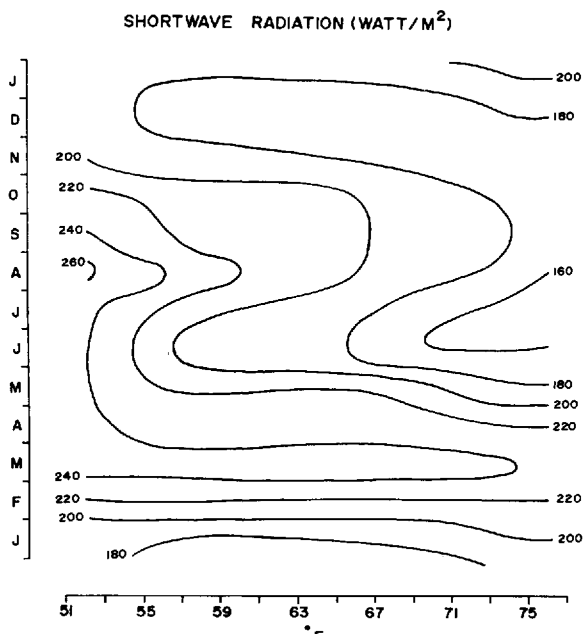

Figure 6. Incoming shortwave radiation (W/m^2).

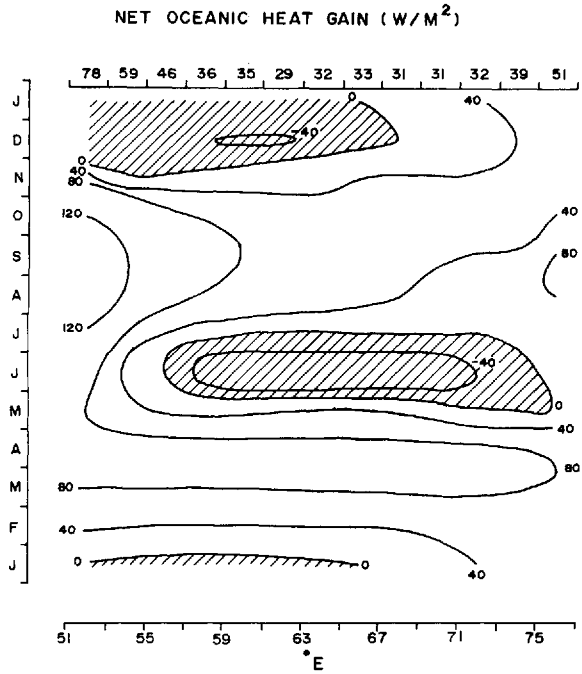

Figure 7. Net oceanic surface heat gain (W/m^2). Hatched portions indicate heat loss. The numbers at the top of the figure give the mean annual heat gain in W/m^2 at each of the 13 areas in Figure 1.

atmospheric boundary layer there more stable. Consequently, convective activity is suppressed leading to less cloudy skies.

At 10N the loss due to latent heat flux is one of the important components of the heat budget. The heat loss is maximum during the SW monsoon. In the month of July, for example, average loss due to the latent heat flux in the middle portion of the 10N strip is approximately 160 W/m^2. It decreases to 120 W/m^2 near the western edge and to about 80 W/m^2 at the eastern end. During the rest of the year there is not much spatial variation, the heat loss on an average is about 80 W/m^2.

The net heat gain at the surface along the 10N is the result of gain due to the shortwave radiation, loss due to the longwave radiation, gain due to the sensible heat and loss due to the latent heat. Of these, the magnitude of the shortwave radiation and of the latent heat are higher than that of sensible heat and of the longwave radiation. Furthermore, the last two do not show much spatial variation. The spatial pattern of the net heat gain shown in Figure 7 is therefore mainly the result of contribution from the shortwave radiation and from the latent heat flux. The rise in heat gain from February to May is due to the increase in the net shortwave radiation. The heat loss seen on the eastern side of the strip during the months of June and July is the result of the heat loss due to the latent heat flux. During these months, even though the western

Table 1. Values assigned to the parameters in the model. ν has been estimated using Charts 17–18 of Krey and Babenerd (1976). η and ϵ_m are taken from Kim (1976).

Parameter	*Value assigned*
ν	0.0006 cm^{-1}
ζ_0	1.026 gm cm^{-3}
$\overline{\alpha}$	2.1×10^{-4} °C^{-1}
g	980 cm^2 s^{-1}
C_p	0.932 cal/(gm °C)
η	1.25
ϵ_m	2×10^{-4} cm^2 s^{-3}

side loses heat due to latent heat flux and due to longwave radiation, the heat gain from sensible heat flux and shortwave radiation, particularly the latter, is sufficient to cause a net heat gain. The heat loss on the western edge during the months of December and January is the result of increase in latent heat loss and decrease in solar radiation. There is a net annual heat gain at the surface by the Arabian Sea. The average heat gain for each of the thirteen areas of the 10N strip is shown in Figure 7.

4. Numerical experiments

Besides the externally specified functions described in the previous section, the following parameters appear in the model equations: ν, ζ_0, $\overline{\alpha}$, g, C_p, η and ϵ_m. Values assigned to these constants are given in Table 1. All numerical experiments were started during mid-February; i.e., at zero hour on the 16th of the month. February was chosen to initiate the experiments because more or less uniform conditions exist in the thermal structure all along the 10N strip at this time. The initial temperature profile had a 80 m homogeneous surface layer of temperature equal to the observed February SST, followed by a temperature discontinuity of 1°C and a region of linear decrease at the rate of 0.06 °C/m (see Fig. 14). The choice of 80 m for the homogeneous surface layer is consistent with the January–February mixed-layer depth in Wyrtki (1971). The temperature discontinuity represents the region of rapid temperature change generally observed below a mixed-layer. The motivation for the choice of 1°C for this discontinuity was that the mixed-layer depth is often taken to be the depth at which temperature decreases by 1°C from the surface temperature (Wyrtki, 1971; Colborn, 1976). The figure of 0.06 °C/m for the temperature change below the mixed-layer is based on the vertical profiles of Levitus (1982). The evolution of the temperature profile for the next 360 days was simulated; each month has been assumed to be of 30 days. The time-step for integrating the equations was fixed at 3 hours, though a figure twice this did not have discernible consequences to the predicted values. We describe below the results of the experiments.

a. Influence of surface fluxes. In the first run the model was forced with surface fluxes alone. The results are shown in Figure 8. Comparing this figure with the observed rate

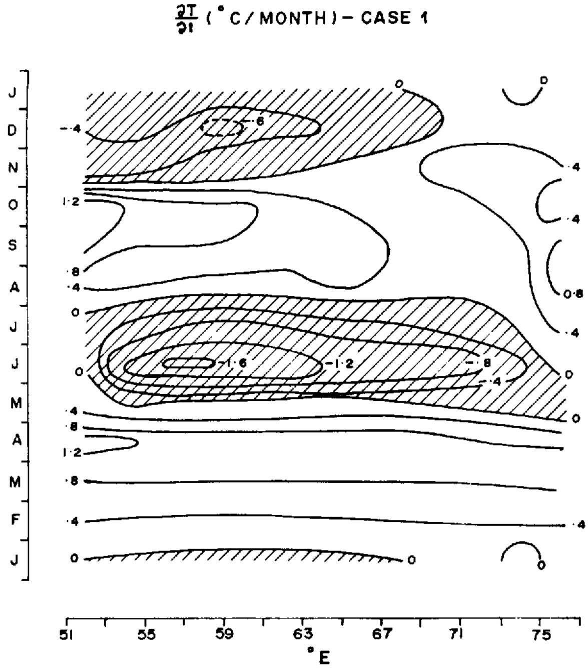

Figure 8. Rate of change of SST (°C/month) simulated by a model forced with surface heat and momentum fluxes.

of change of SST, Figure 4, we see that from mid-February to the end of April the predicted and the observed values are in good agreement. The behavior of the mixed-layer in the model during this period was characterized by a shallowing mixed-layer due to detrainment, and a rapid increase in SST. The decrease in wind stress during January–April led to detrainment. As a result, the heat gained across the air-sea interface got restricted to continuously shallowing depths. This led to increased stratification which made it harder for the wind to stir the water. As the decrease in wind stress was larger on the western side, so was the shallowing. On the west (east) the mixed-layer depth decreased to about 50 m (55 m). These values are consistent with the mixed-layer depths given in Wyrtki (1971).

The success of the model in simulating the conditions during the pre-monsoon warming phase was not repeated during the SW monsoon cooling. Simulations did predict, in agreement with the observations, a decrease in SST. There were, however, the following differences. First, the observed rate of cooling has two maxima, both located in coastal areas. The simulated rate of cooling had a maximum in the mid-sea area. Second, the overall predicted magnitude of cooling is weaker than the observed one. And third, the predicted duration of cooling is shorter than the observed duration. We see below that the main cause for these differences is the neglect of the advective field.

In the model run, the decrease in the SST occurred due to two factors. The more important of these was the entrainment of the cooler deeper water following the onset of the SW monsoon. The other cause of cooling was the loss of heat at the surface. Though the wind stress has a maximum on the western side, the rate of cooling was not maximum there, because a high influx of shortwave radiation and a net heat gain at the surface kept low the rate of cooling. The maximum instead occurred farther offshore, at about 56E which experiences a net surface heat loss.

The coast of Somalia (Schott, 1983) and the southwest coast of India (Shetye, 1984) are known to experience upwelling during the SW monsoon. Its importance to the SST variability can be seen in Figure 4 which shows a tongue-like feature protruding offshore from the coastal region. The absence of such a feature in Figure 8 is due to the neglect of the advective field. The need for including upwelling also became clear because the mixed-layer in the coastal areas kept deepening with the onset of the monsoon, in contrast to the shallowing reported in the observations.

The model performed better in the offshore areas. The spatial pattern of the predicted rate of change of SST is in fair agreement with Figure 4. The observed gradient in SST the mid-Arabian Sea seen soon after the onset of the monsoons can therefore be attributed, at least partly, to the eastward reduction in the wind stress. In the mid-sea area the model predicted an increase in the depth of the mixed-layer from around 70 m during May-end to almost 120 m toward the end of August. The latter is about 20% larger than the observed figure. The magnitude of the predicted rate of cooling in the mid-sea is lower than the observed. As we shall see later this is very likely due to neglect of horizontal advection.

As the southwest monsoon withdraws, the wind stress drops and the surface heat gain increases. Under the combined influence of these two, in the model run the SST rose and the mixed-layer got shallower. By the end of the warming season, the simulated h in the mid-sea region was approximately 70 m. This, as well as the predicted rate of change of temperature is consistent with observations. The August–November warming phase is thus very much like the February–May phase, the mixed-layer processes in both cases being controlled by the surface fluxes alone.

With the onset of the northeast monsoon the winds increase. Off Somalia, the stress increases from 0.1 dyne/cm^2 to approximately 1 dyne/cm^2. A marginal increase also occurs on the eastern side. The distribution of net heat flux shows a loss of heat on the western side and a gain on the eastern side. In the model run, on the western side the mixed-layer deepened and the SST decreased. On the eastern edge, because the increase in wind stress is marginal the model showed only a small increase in the mixed-layer depth. The cooling of the surface layer due to entrainment was, however, offset by the net heat gain at the surface. The result was a small increase in the SST. The discrepancy between the model predictions and the observations on the eastern side can be attributed to uncertainties in the parameters built into the model. It was noticed that because the magnitudes of both the predicted warming and the observed cooling are weak, a small change in a parameter such as ν could increase the rate of

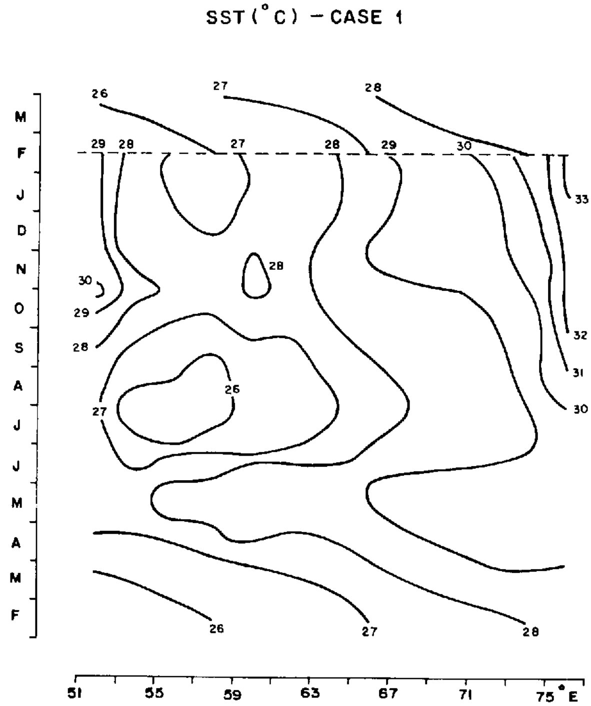

Figure 9. SST (°C) simulated by a model forced with surface heat and momentum fluxes.

entrainment sufficiently so that there would be a decrease in the SST instead of the increase seen in Figure 8.

So far in the discussion we have focussed on a comparison between the predicted and the observed rate of change of SST. Let us now compare the predicted and the observed SST. The simulated temperature field is shown in Figure 9. From the figure we note that by the end of the annual cycle each of the areas in the 10N strip underwent a net increase in SST. The difference between the initial temperature and the temperature a year later, was higher, 5°C, in the coastal areas than in the open-sea areas where it was 2°C. The reason behind the temperature rise is easy to see. The 10N strip is a region of net annual heat gain. In the model run, there was no mechanism to remove this heat from the water column and to ensure that the column had the same heat at the end of the annual cycle as at the beginning of it. In the absence of such a mechanism the heat of the water column rose from month to month by an amount equivalent to the heat gained during the month. Coastal areas gain more heat so the temperature jump was higher there. The slow accumulation of heat is not of serious concern to compute the SST on a time-scale short in comparison to the annual cycle. However, to simulate the behavior of the AS on an annual time scale the mechanism for the removal of heat has to be identified. Horizontal advection is a likely candidate.

In summary, we see that a model forced with surface fluxes alone performs well,

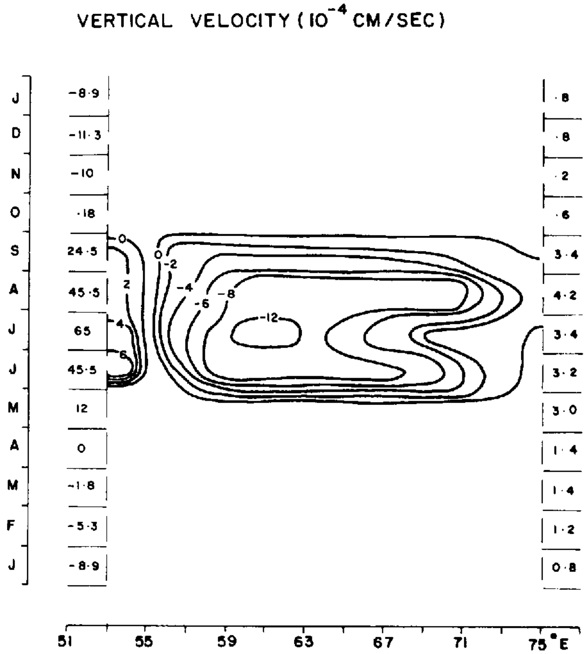

Figure 10. Vertical velocity field below the mixed-layer (10^{-4} cm/s). For coastal regions (Areas 1 and 13 in Fig. 1) the monthly-mean values of the vertical velocity are shown by discrete numbers. A negative (positive) value of the velocity implies downwelling (upwelling). In the open-sea the velocity is non-zero only from June through September.

except during the SW monsoon when the advective contribution to the SST change is expected to be significant. In the remaining part of this section we examine the impact of vertical and horizontal advection on the AS mixed-layer.

b. Influence of vertical advection. The main difficulty in incorporating the influence of the vertical velocity in the model is the determination of the velocity field. For areas 2–12, the deep sea region, we take

$$w = \frac{1}{\zeta_0 f} \text{curl}\, \tau \tag{5}$$

f being the Coriolis parameter. Hantel (1970) has described the annual cycle of the curl of wind stress over the Indian Ocean. In the Arabian Sea the period of high curl lasts only from June to September. The wind circulation over the AS during this period is marked by the presence of a low level jet (Findlater, 1971). Off Somalia, the resulting surface wind has a maximum located a few longitude-degrees east of the coast. This produces an intense field of curl of the wind stress, which is positive just off the coast, vanishes at the axis of the jet and is negative over the area east of it. The vertical velocity computed by using Hantel's values for the curl in Eq. (5) is shown in Figure 10. The contours in the figure show upwelling in a narrow band just off the

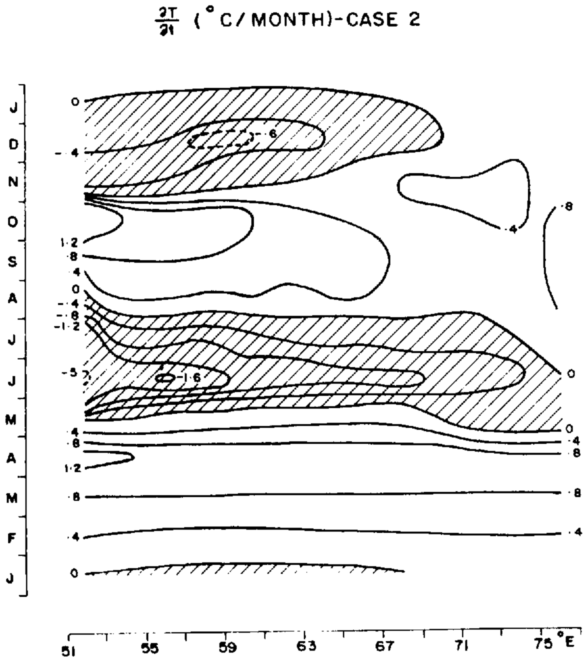

Figure 11. Rate of change of SST (°C/month) simulated by a model forced with surface fluxes and with the prescribed vertical velocity field below the mixed-layer.

coast of Somalia. Note that this is due to the positive curl of the wind stress over this band and not due to coastal processes. Downwelling arising due to a negative curl of wind stress persists over the rest of the strip. The magnitude of the wind stress curl from October to May is sufficiently weak to set w equal to zero.

For the coastal area (Areas 1 and 13) we assume

$$w = \frac{\tau_l}{fR} \tag{6}$$

where τ_l is the longshore component of wind stress. The equation above follows from simple mass balance considerations. (τ_l/f) is the offshore Ekman transport. We assume that this is compensated by a vertical transport with velocity w averaged over an offshore distance R. We take R to be 200 km—the approximate offshore extent of Areas 1 and 13. The monthly-mean values of w thus computed are shown in Figure 10. We note that Schott and Quadfasel (1982) inferred a vertical velocity of 60×10^{-4} cm/s at 130 m near 6–8N in June 1979. Though the longshore component off the southwest coast of India is weaker than that off Somalia, it remains conducive to upwelling throughout the year.

Figure 11 gives the rate of change of temperature computed by using the model forced with surface fluxes and with w in Figure 10. As before the run was initiated on 16 February. The behavior of the mixed-layer in the run remained identical to the earlier case till the end of April. During May, due to the influence of upwelling off Somalia, Area 1 showed a weak cooling of 0.1°C/month. In the open sea, during the SW monsoon, downwelling pushed the thermocline deeper and increased the depth of the homogeneous surface layer. As a result, the effect of surface cooling got distributed over a larger volume, thereby reducing the decrease in SST. The difference in the rate of cooling with downwelling versus that without downwelling was small, typically of the order of 0.2–0.3°C/month. Over Areas 2 and 3, where upwelling occurs because of a positive wind stress curl, the rate of cooling increased by about 0.2°C/month and the mixed-layer got shallower by about 15 m/month.

The upwelling in Area 13 was too weak to have any significant impact on the surface temperature distribution. The situation off the coast of Somalia was just the opposite. Here the upwelling enhanced cooling by such a large magnitude that by the end of August the SST had dropped to 4°C, clearly an unphysical result. The reason for this is easy to see. With the vertical velocity shown in Figure 10, and a vertical temperature gradient of 0.06°C/m, the rate of cooling due to vertical advection, $-w\ (\partial T/\partial z)_{-h}$, at a point just below the mixed-layer is about 7°C/month. This explains why the SST dropped to 4°C by the end of August. To avoid the cooling of this magnitude, for the run whose results are shown in Figure 11, the temperature gradient $(\partial T/\partial z)_{-h}$ was reduced to 0.006°C/m in July. This value is lower by a factor of 10 than the one used elsewhere. The rationale behind this is that the vertical temperature gradient, more than 200 m below the mixed-layer, is generally much lower than the one observed just below the mixed-layer. This, however, is strictly an adhoc remedy. It does not alleviate the real problem which is that the one-dimensional model used here is inadequate to handle the complex conditions that exist off the Somali coast during the SW monsoon (see Schott (1983) for a review). The dynamics of the coastal circulation has to be incorporated into a model aimed at realistic simulation of the SST along the coast during the SW monsoon.

c. Influence of horizontal and vertical advection. The quantity relevant to the estimation of the cooling due to the horizontal advection is $\mathbf{u} \cdot \nabla T_s$. Monthly-mean ship-drift estimates in the N. Indian Ocean have been described in the KNMI Atlas (1952) on a 2°-latitude by 2°-longitude grid. Figure 12 shows the annual march of the drifts over the 2-degree-latitude strip from 10N to 12N and stretching from the coast of Somalia to that of India. A smoothed value of the drift was used to compute $\mathbf{u}$. The velocity in Area 6, for example, was computed by averaging vectorially the surface drifts from the KNMI Atlas (1952) in the four 2°-squares that surround Area 6 (see Fig. 1). The computed values of $\mathbf{u} \cdot \nabla T_s$ are shown in Figure 13, T_s being the observed monthly-mean SST taken from HL1. The figure suggests that the advective influence is expected to play a significant role in controlling the SST only from June to September. During the rest of the year the magnitude of $\mathbf{u} \cdot \nabla T_s$ is very much smaller than the observed rate of change in SST. This observation compliments our earlier conclusion that except during the southwest monsoon season the mixed-layer processes along the 10N strip are dominated by the surface fluxes alone.

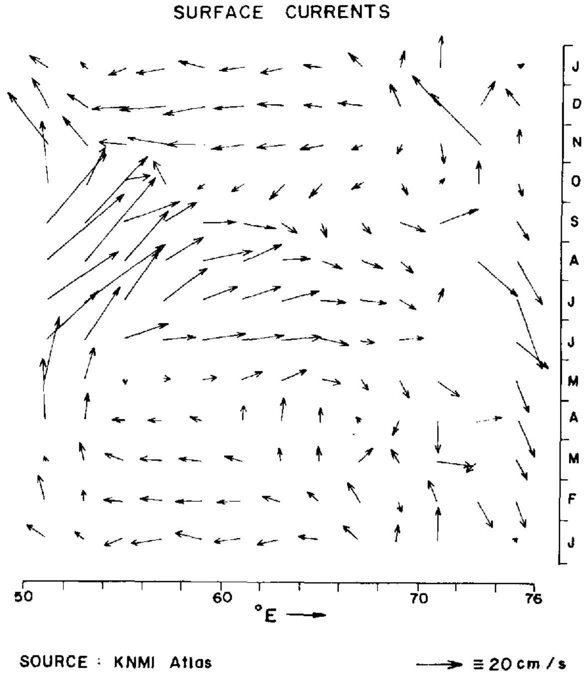

Figure 12. Ship-drift estimates along a zonal strip with the meridional extent of 10–12N. Each arrow gives monthly-mean estimate over a two-degree-latitude by two-degree-longitude area. The figure is based on the KNMI Atlas (1952).

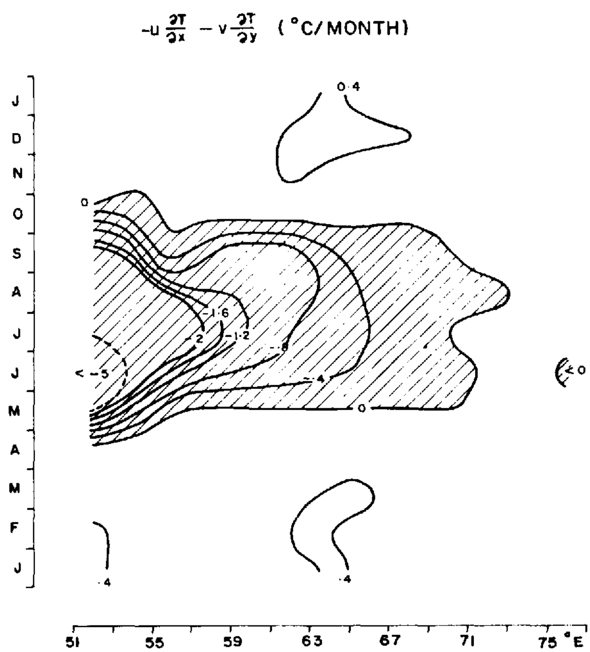

Figure 13. Estimate of $-\mathbf{u} \cdot \nabla T_s$. See section 4.3 for the method of computation.

The numerical experiments with w and $\mathbf{u} \cdot \nabla T_s$ included in the model have not been carried out for the entire strip. Instead, attention was restricted to only one open-ocean region, Area 6, and the kind of changes that the vertical and horizontal advection brought about on the thermal structure of the upper ocean were examined. The results are summarized in Figure 14. In case A, the model was forced with surface fluxes alone. In B, surface fluxes and vertical advection were included. Case C considered the influence of all three–surface fluxes, and horizontal and vertical advection. Each run was initiated on 16 February, with identical vertical temperature profiles. It is noted that Figure 16 in Colborn (1976) gives the annual march of the upper ocean thermal structure in the southeast AS, a region which covers Area 6 in the 10N strip.

All the three cases in Figure 14 show a similar evolution till the end of May. Until April, the mixed-layer behavior was marked by formation of a progressively shallower surface turbulent regime. The shallowing occurred in steps because of the sudden changes in heat and momentum fluxes from one month to the next. During May, the mixed-layer deepened, but only slightly, due to increase in wind stress. From June onward, the temperature structure evolved differently for the three cases. For the model forced with surface fluxes alone, the deepening of the mixed-layer was due to entrainment alone. When the vertical velocity is imposed the deepening is enhanced because of the downwelling. The apparent rise in the heat content of the upper ocean that the temperature structure in case B implies is artificial. Any downwelling has to be accompanied by horizontal convergence of mass. The contribution of the horizontal movement of mass to the temperature variation is determined by $\mathbf{u} \cdot \nabla T_s$. Its neglect is the cause of the apparent rise in heat seen in case B.

The contribution of $\mathbf{u} \cdot \nabla T_s$ has been taken into account in case C. The $\mathbf{u}$ field based on ship-drift estimates is a reasonable indicator of the currents in the surface mixed-layer, but it gives no information on the currents in the deeper layers. It is expected that the deeper currents are much weaker, and hence the magnitude of the advective cooling there should be much weaker than $-\mathbf{u} \cdot \nabla T_s$ computed by using the surface currents. The rate of advective cooling in the "deeper region" was therefore set equal to zero, after assuming that it is the region where the temperature is less than the SST minus one degree centigrade. The choice of one degree is arbitrary, but was made for the lack of a better alternative.

The results summarized in Figure 14 show that one of the important roles that the advection plays during the SW monsoon is the export of heat that the water column gains at the surface during the course of a year. In case C, by the end of the southwest monsoon season, the SST is the lowest of all the three cases, and the SST more or less returns to the initial (February 16) value at the end of the annual cycle. In the model run not all the heat was, however, exported. Some of it was transferred to the deeper layers. The main contributing factor to this was the vertical transfer of heat due to the downwelling during the SW monsoon. There is some evidence in the climatic data to support such a vertical heat transfer. Levitus (1982) has given the mean vertical temperature structure up to a depth of 250 m during the four seasons of the year on a

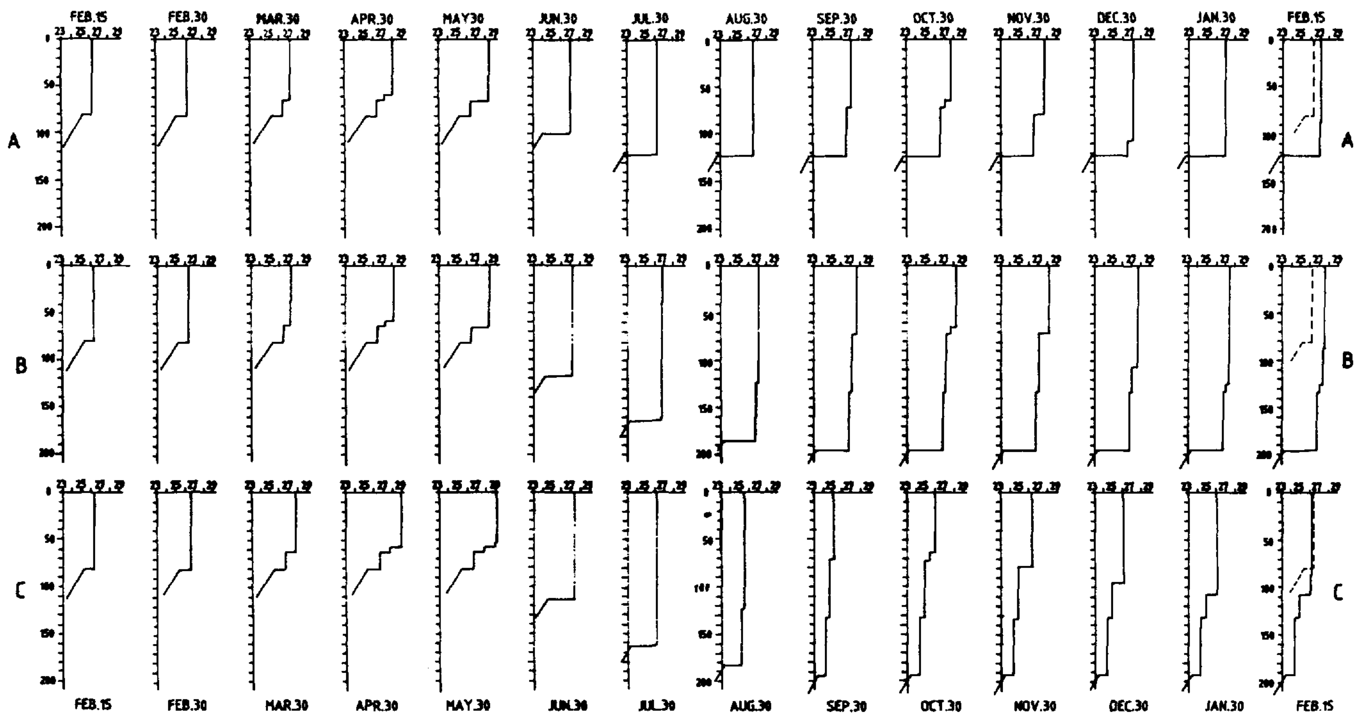

Figure 14. Annual march of the computed temperature profiles for Area 6 in Figure 1. Case A (top row) shows the temperature profiles computed by using the model with the surface fluxes alone. In case B (middle row) the vertical advection has been taken into account in addition to the surface fluxes. In case C (bottom row) all the three—surface fluxes, and horizontal and vertical advection—are taken into account. The initial (February 15) profiles are identical for the three cases. In the row on the extreme right of the figure the dashed line gives the initial profile.

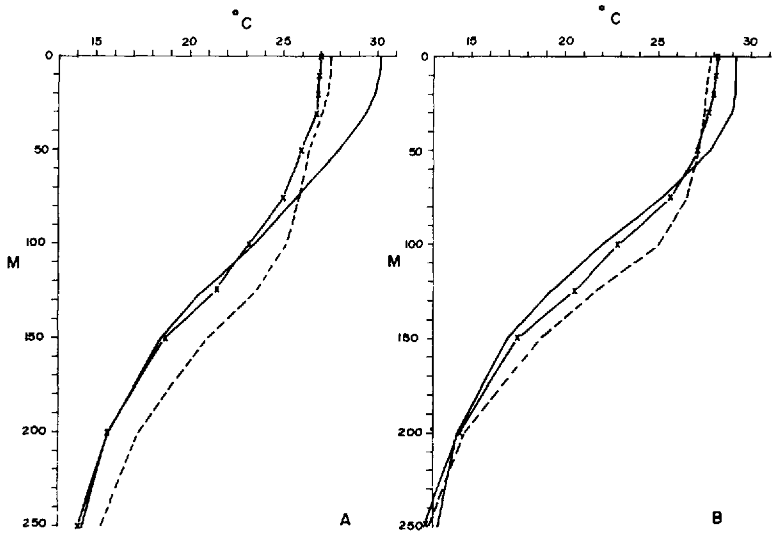

Figure 15. Seasonal mean vertical temperature profiles in the Arabian Sea. (A) refers to the square 10–15N and 60–65E; (B) refers to the square 5–10N and 60–65E. Spring (May, June, July) profiles are shown by —, Summer (Aug., Sept., Oct.) by ----- and Fall (Nov., Dec., Jan.) by —x—x—. The vertical axis gives depth in m. Source of data: Levitus (1982).

5°-longitude by 5°-latitude grid. In Figure 15 we have plotted the temperature profiles given by him for three seasons: spring (May, June and July), summer (Aug., Sept. and Oct.) and fall (Nov., Dec. and Jan.). Though the three-month averages plotted in the figures are not ideally suited to describe changes in the water column during the SW monsoon, they do bring out an interesting aspect. From spring to fall, the profiles show a decrease in the temperature near the surface, but an increase below the depth of approximately 75 m. The near surface heat loss can be attributed to entrainment, to heat loss due to air-sea fluxes and to advective cooling. The increase in temperature in the deeper layers is very likely related to downwelling. Both the 5°-squares for which data have been given in Figure 15, lie in the area of negative wind stress curl. If the spring profile below the depth of about 75 m is moved down by about 25 m, then it would lie close to the summer profile. Such a movement could be caused by a downwelling velocity of 3×10^{-4} cm/s, a figure consistent with our estimate of the vertical velocity field shown in Figure 10. At the present it is not known how the heat transferred to the deeper layers gets removed from the AS.

5. Concluding comments

The numerical experiments reported here were plagued with uncertainties both in forcing functions and in model parameters. Furthermore, the model was found to be inadequate to handle the coastal region during the SW monsoon. In spite of these limitations it did allow a synthesis of different pieces of available data (monthly-mean air-sea fluxes, horizontal advection, etc.) into a comprehensive picture of the annual cycle of the ASST. Though this model provides strictly a "zero-order" description of the ASST variability, it permits some useful inferences.

The first conclusion we draw is that the influence of the surface heat and momentum fluxes alone dominates the AS mixed-layer processes during the following three of the four warming/cooling phases: the February–May warming phase; the post-monsoon, September–November, warming phase; and, the northeast monsoon, November–January, cooling phase. This implies that during the nine months of a year the ASST variability can be modelled reasonably well with equations that include the Kraus-Turner thermodynamics alone.

The second conclusion is that to model the ASST during the SW monsoon it is necessary to consider both thermodynamics and dynamics. The latter control the advective field which has the following influences on the open-sea SST:

(a) Upwelling/downwelling: Upwelling due to positive wind stress curl enhances cooling. Downwelling has only marginal effect on SST variation. It, however, influences the vertical distribution of heat by pushing down the thermocline.

(b) Horizontal advection: An energetic surface circulation and strong temperature gradients combine to contribute significantly to the SST change during the SW monsoon. The surface circulation helps to remove a major fraction of the heat that the water column gains from air-sea fluxes during the course of a year.

Dynamics of the circulation off Somalia have received considerable attention (Schott, 1983). In contrast, little is known about the rest of the basin. Our results suggest that it will not be possible to simulate the ASST realistically during the SW monsoon unless both thermodynamics and dynamics are adequately modelled. This conclusion should be of interest in experiments with Atmospheric General Circulation Models which have attempted to study the role of ASST in the behavior of the monsoon over India (Druyen, 1983).

At the present a major obstacle in making further progress in understanding the ASST is the lack of reliable time-series data on air-sea fluxes and on subsurface temperature and salinity distribution. Such data, which have been routinely collected by weather ships in the North Atlantic and in the North Pacific, are needed to address many of the details that have been ignored here. Observations are also needed to determine some of the model parameters. Prominent amongst these is the coefficient of extinction, ν, which depends on many factors including biological productivity and turbidity, and which greatly influences the depth of the mixed-layer.

Acknowledgments. Dr. E. Desa and his colleagues in the Marine Instrumentation Division went out of their way to make computer facilities available during the study. Ravindranath Uchil drafted the figures. The paper has benefitted from comments of Drs. P. Desai, S. Gadgil, J. S. Sastry and S. Satyandranath, and from the suggestions of the reviewers.

REFERENCES

Alexander, R. C. and J. W. Kim. 1976. Diagnostic model study of mixed-layer depths in the summer north Pacific. J. Phys. Oceanogr., *6,* 293–298.

Colborn, J. 1976. The Thermal Structure of the Indian Ocean. The University Press of Hawaii, 173 pp.

Denman, K. 1973. A time-dependent model of the upper ocean. J. Phys. Oceanogr., *3*, 173–183.

Denman, K. and M. Miyake. 1973. Upper layer modification at ocean station "Papa": Observations and simulation. J. Phys. Oceanogr., *3*, 185–196.

Druyan, L. M., J. Miller and G. Russel. 1983. Atmospheric general circulation model simulations with an interactive ocean: effect of SST anomalies in the Arabian Sea. Atmos.-Ocean, *21*, 94–106.

Duing, W. and A. Leetmaa. 1980. Arabian Sea cooling: a preliminary heat budget. J. Phys. Oceanogr., *10*, 307–312.

Findlater, J. 1971. Mean monthly airflow at low levels over the Western Indian Ocean. Geophys. Mem., *115*, 53.

Gill, A. and J. Turner. 1976. Comparison of seasonal thermocline models with observations. Deep-Sea Res., *23*, 391–401.

Hantel, M. 1970. Monthly charts of surface wind stress curl over the Indian Ocean. Mon. Weath. Rev., *98*, 765–773.

Hastenrath, S. and P. Lamb 1979a. Climatic Atlas of the Indian Ocean, Part 1: Surface Climate and Atmospheric Circulation. The University of Wisconsin Press.

—— 1979b. Climatic Atlas of the Indian Ocean, Part II: Heat Budget. The University of Wisconsin Press.

Kim, Jeong-Woo. 1976. A generalized bulk model of the oceanic mixed-layer. J. Phys. Oceanogr., *6*, 686–695.

Kondo, J. 1975. Air-Sea bulk transfer coefficients in diabatic conditions. Boundary Layer Meteor., *9*, 91–112.

Koninklijk Nedelands Meteorologisch Institut. 1952. Indische Ocean Oceanografische an Meteorologisch Oegevens, Second Edition, Publication 132, 24 charts.

Kraus, E. and J. Turner. 1967. A one dimensional model of the seasonal thermocline II: The general theory and its consequences. Tellus, *19*, 98–106.

Krey, J. and B. Babenerd. 1976. Phytoplankton Production Atlas of the International Indian Ocean Expedition. I.O.C., UNESCO, Paris.

Levitus, S. 1982. Climatological Atlas of the World Oceans. NOAA Professional Paper 13, U.S. Govt. Printing Office, Washington D.C.

Schott, F. 1983. Monsoon response of the Somali Current and associated upwelling. Progr. Oceanogr., *12*, 357–381.

Schott, F. and D. R. Quadfasell. 1982. Variability of the Somali current system during the onset of the southwest monsoon 1979. J. Phys. Oceanogr., *12*, 1343–1357.

Shetye, S. R. 1984. Seasonal variability of the temperature field off the south-west coast of India. Proc. Indian Acad. Sci. (Earth and Planet. Sci.), *93*, 399–411.

Shukla, J. 1975. Effect of Arabian sea surface temperature anomaly on Indian summer monsoon: a numerical experiment with GFDL model. J. Atmos. Sci., *32*,503–511.

US Navy Marine Climatic Atlas of the World Ocean. 1976. U.S. Government Printing Office, Washington D.C.

Washington, W., R. Chervin and G. Rao. 1977. Effect of a variety Indian Ocean surface temperature patterns on the summer monsoon circulation: experiment with NCAR GCM. Pure and Appl. Geophys., *115*, 1335–1356.

Wyrtki, K. 1971. Oceanographic Atlas of the International Indian Ocean Expedition. U.S. Government Printing Office, Washington D.C.

Received: *1 November, 1985;* revised: *12 May, 1986.*